MOLECULAR AND CELLULAR BIOLOGY, June 2008, p. 4026–4039 Vol. 28, No. 12
0270-7306/08/$08.00+0 doi:10.1128/MCB.02062-07
Copyright © 2008, American Society for Microbiology. All Rights Reserved.

Emilin1 Deficiency Causes Structural and Functional Defects of Lymphatic Vasculature[▽]

Carla Danussi,[1] Paola Spessotto,[1] Alessandra Petrucco,[1] Bruna Wassermann,[1] Patrizia Sabatelli,[2] Monica Montesi,[3] Roberto Doliana,[1] Giorgio M. Bressan,[3] and Alfonso Colombatti[1,4,5]*

Division of Experimental Oncology 2, Department of Molecular Oncology and Translational Research, CRO-IRCCS, Aviano, Pordenone, Italy[1]; IGM-CNR, Unit of Bologna c/o IOR, Bologna, Italy[2]; Mouse Genetics Laboratory, Department of Histology Microbiology and Medical Biotechnologies, University of Padua, Padua, Italy[3]; Department of Biomedical Sciences and Technologies, University of Udine, Udine, Italy[4]; and MATI Center of Excellence, University of Udine, Udine, Italy[5]

Received 16 November 2007/Returned for modification 25 December 2007/Accepted 27 March 2008

Lymphatic-vasculature function critically depends on extracellular matrix (ECM) and on its connections with lymphatic endothelial cells (LECs). However, the composition and the architecture of ECM have not been fully taken into consideration in studying the biology and the pathology of the lymphatic system. EMILIN1, an elastic microfibril-associated protein, is highly expressed by LECs in vitro and colocalizes with lymphatic vessels in several mouse tissues. A comparative study between WT and *Emilin1*$^{-/-}$ mice highlighted the fact that *Emilin1* deficiency in both CD1 and C57BL/6 backgrounds results in hyperplasia, enlargement, and frequently an irregular pattern of superficial and visceral lymphatic vessels and in a significant reduction of anchoring filaments. *Emilin1*-deficient mice also develop larger lymphangiomas than WT mice. Lymphatic vascular morphological alterations are accompanied by functional defects, such as mild lymphedema, a highly significant drop in lymph drainage, and enhanced lymph leakage. Our findings demonstrate that EMILIN1 is involved in the regulation of the growth and in the maintenance of the integrity of lymphatic vessels, a fundamental requirement for efficient function. The phenotype displayed by *Emilin1*$^{-/-}$ mice is the first abnormal lymphatic phenotype associated with the deficiency of an ECM protein and identifies EMILIN1 as a novel local regulator of lymphangiogenesis.

Lymphatic and blood vascular systems have distinct structural characteristics that reflect their specific and complementary functions. The lymphatic vasculature represents a second circulatory system and maintains tissue fluid homeostasis; it plays a major role in the absorption of dietary fat and in immune response, transporting lymphocytes and antigen-presenting cells to regional lymph nodes; finally, it provides routes for tumor metastasis (8). The lymphatic system consists of a complex network of lymphatic capillaries, which are uniquely adapted for the uptake of protein-rich lymph from tissue interstitium, and collecting lymphatic vessels that transport lymph back to the blood vascular system. The latter are surrounded by a basement membrane and smooth muscle cells, which are less organized than in blood vessels and, in addition, have intraluminal valves, which prevent lymph backflow (26). By contrast, lymphatic capillaries are blind-end vessels, lined by a single thin layer of overlapping lymphatic endothelial cells (LECs) directly connected to the surrounding extracellular matrix (ECM) by means of anchoring elastic filaments (18). These structures play a fundamental role in lymphatic-vessel function and represent one of the main distinguishing features between lymphatic and blood capillaries. When interstitial fluid pressure increases, anchoring filaments exert tension on LECs, thereby widening the capillary lumen and opening the overlapping cell junctions, which enable fluid and macromolecule uptake and cell entry. It is thought that abnormalities of anchoring filaments may reduce adsorption from the interstitium and propulsion of lymph and cells and promote pathological conditions, such as lymphedema or diseases related to impaired immune responses (9, 18). Furthermore, the perivascular ECM plays an integral role in lymphatic-vessel function, as the fluid equilibrium is controlled by the cooperation of both lymphatic function and the ECM (40). The elasticity and hydration of a tissue is determined by the composition and organization of the ECM. Extensive and chronic degradation of the ECM eventually renders lymphatic vessels nonresponsive to the changes in the interstitium and therefore causes dysfunction (28, 30).

Lymphatic and blood endothelial cells express different lineage-specific molecules involved in the regulation of their biological functions that are frequently used as distinguishing markers, such as vascular endothelial growth factor receptor 3 (VEGFR-3) (22), podoplanin (3), Prox-1 (44), LYVE-1 (1, 34), neuropilin 2 (46), CCL21 (24), and desmoplakin (12). Recently, a comparative microarray analysis of gene expression profiles of lymphatic and blood endothelial cells identified previously unknown lymphatic lineage genes, including macrophage mannose receptor 1, plakoglobin, the chemokine CCL20, the integrin $\alpha 9\beta 1$ (19, 32), and EMILIN1 (33).

EMILIN1 is an ECM glycoprotein associated with elastic fibers (4, 6) and composed of an N-terminal cysteine-rich domain and the EMI domain (11), followed by a coiled-coil structure, a short collagenous stalk, and a C-terminal gC1q

* Corresponding author. Mailing address: Division of Experimental Oncology 2, Department of Molecular Oncology and Translational Research, CRO-IRCCS, via F. Gallini 2, 33081 Aviano, Pordenone, Italy. Phone: 39 0434 659 365. Fax: 39 0434 659 428. E-mail: acolombatti@cro.it.

▽ Published ahead of print on 14 April 2008.

domain (7). EMILIN1 is particularly abundant in the walls of large blood vessels, such as the aorta (10), and has been implicated in multiple functions. EMILIN1 is involved in elastogenesis and in the maintenance of blood vascular cell morphology (48). It interacts with the $\alpha4\beta1$ integrin through the gC1q1 domain (36) and has strong adhesive and migratory properties for different cell types (10, 36, 37). EMILIN1, via the EMI domain, regulates pro-transforming growth factor beta (TGF-β) maturation and is involved in blood pressure homeostasis (47).

To directly investigate the physiological function of EMILIN1 in lymphatic vessels, we studied the effects of its absence in mice that had targeted deletions in the *Emilin1* gene (48). Here, we report that EMILIN1 is highly expressed by LECs in vitro and that it colocalizes with lymphatic vessels in several mouse tissues. Importantly, *Emilin1* deficiency results in hyperplasia and enlargement of lymphatic vessels and in a significant reduction of anchoring filaments compared to those of wild-type (WT) mice. The lymphatic vessels of *Emilin1*$^{-/-}$ mice are functionally altered. We found that lack of EMILIN1 leads to a mild lymphedema associated with inefficient lymph drainage and increased leakage. In addition, *Emilin1*$^{-/-}$ mice develop larger lymphangiomas than their WT littermates. Altogether, these findings demonstrate an important role of EMILIN1 in the structure-function relationship of lymphatic vessels and identify EMILIN1 as a lymphangiogenesis modulator.

MATERIALS AND METHODS

Antibodies. Rabbit polyclonal anti-mouse and -human VEGFR-3 (Santa Cruz Biotechnology, Santa Cruz, CA), rat monoclonal anti-mouse VCAM-1 (Chemicon International, Temecula, CA), rabbit polyclonal anti-human LYVE-1 (Upstate, Lake Placid, NY), rabbit polyclonal anti-human Prox-1 (Abcam, Cambridge, United Kingdom), mouse monoclonal anti-human D2-40 (podoplanin; Signet Laboratories, Dedham, MD), and mouse monoclonal anti-human CD31 (Chemicon International) antibodies were used for mouse and human LEC characterization. For lymphatic-vessel detection, a rabbit polyclonal anti-mouse LYVE-1 antibody (Abcam) and a hamster monoclonal anti-mouse podoplanin antibody (Abcam) were used. For blood vessel detection (5), the supernatant of a rat monoclonal anti-mouse multimerin 2 (MMRN2; previously named endoGlyx-1, clone 2063E2A11) produced in our laboratories was used. The rat monoclonal anti-mouse EMILIN1 antibody (clone 1007C11A8) was also produced in our laboratories. The rabbit polyclonal anti-Ki67 proliferation marker was purchased from Abcam.

Mouse procedures and cell culture. Procedures involving animals and their care were conducted according to institutional guidelines in compliance with national laws (D.Lgs. no. 116/92). *Emilin1*$^{-/-}$ mice (CD1 and C57BL/6 strains) were generated as previously described by Zanetti et al. (48). For lymphangioma induction, the protocol published by Mancardi et al. (27) was followed using BALB/c (Harlan Italy S.r.L., Udine, Italy) and CD1 mice. Briefly, the mice were intraperitoneally injected twice, with a 15-day interval, with 200 μl of emulsified (1:1 with PBS) incomplete Freund's adjuvant (Sigma, St. Louis, MO). Hyperplastic vessels were isolated from the liver and diaphragm after day 30 and treated with 0.5 mg/ml collagenase A (Roche Diagnostics, Monza, Italy), and the resulting single-cell suspension was cultured as previously described (27). After 7 to 10 days of culture, subconfluent cells (lymphangioma-derived endothelial cells [LAECs]) were recovered with trypsin/EDTA and characterized by immunocytochemistry.

Human microvascular endothelial cells dermal lymphatic-neonatal (HMVEC-dLyNeo), HMVEC lung lymphatic (HMVEC-LLy), and the media optimized for their growth (EGM-2 MV) were purchased from Cambrex Bio Science (Verviers, Belgium); bEnd3, a mouse endothelioma cell line derived from brain capillaries, was from ATCC (Manassas, VA). Human umbilical vein endothelial cells (HUVEC) were isolated from three to five normal umbilical cord veins by collagenase digestion following the standard procedure previously described (25).

Immunofluorescence and whole-mount staining. Mouse tissues were excised, embedded in OCT (Kaltek, Padova, Italy), snap-frozen, and stored at −80°C. Cryostat sections (7 μm) were air dried at room temperature and kept at −80°C wrapped in aluminum foil. Before being used, the sections were equilibrated at room temperature, hydrated with phosphate-buffered saline (PBS) for 5 min, and fixed with PBS–4% paraformaldehyde (PFA) for 15 min. Then, the sections were permeabilized (with PBS, 1% bovine serum albumin, 0.1% Triton X-100, 2% fetal calf serum) for 5 min and saturated with the blocking buffer (PBS, 1% bovine serum albumin, and 2% serum) for 30 min. The primary antibodies were then incubated at room temperature for 1 h, followed by three 5-min washes in PBS and secondary-antibody incubation for 1 h. Multiple staining was performed using a combination of differently conjugated secondary antibodies: Alexa Fluor 488, Alexa Fluor 568, and Alexa Fluor 633 (Molecular Probes, Eugene, OR). Nuclei were visualized with propidium iodide or ToPro, both from Molecular Probes.

For whole-mount staining, mice were anesthetized with 0.4 g Avertin (Sigma)/kg of body weight, perfused with PBS PFA 1%, and sacrificed. Tissue specimens of interest were finely minced and fixed in 4% PFA for 18 h at 4°C. Then, the blocking solution (PBS, 0.3% Triton X-100, and 5% serum) was added for 8 h at 4°C, followed by primary-antibody incubation for 18 h at 4°C. After five washes with PBS 0.3% Triton X-100, the secondary antibody was added, and the specimens were incubated for 18 h at 4°C. Images were acquired with a Leica TCS SP2 confocal system (Leica Microsystems Heidelberg, Mannheim, Germany), using Leica confocal software.

Electron microscopy. Skin fragments were dissected from 12-week-old mice, fixed with 2.5% glutaraldehyde in 0.1 M sodium cacodylate buffer (pH 7.4) overnight, washed in 0.1 M sodium cacodylate buffer overnight, and treated with 2% tannic acid in 0.1 M sodium cacodylate buffer as previously described (48). All samples were dehydrated with ethanol and embedded in Epon E812. Ultrathin sections were obtained from several blocks, stained with lead citrate and uranyl acetate, and observed in a Philips EM 400 transmission electron microscope operated at 100 kV.

In vitro tube formation assay. To assess the ability of mouse LAECs to form vessel-like structures in vitro, Matrigel (8.8 mg/ml; BD Biosciences, Erembodegem, Belgium) was added to the wells of a 96-well plate in a volume of 50 μl and allowed to solidify for 30 min at 37°C. Once it was solid, 2×10^5 LAECs were seeded in each well in 200 μl of EGM-2 MV medium and incubated at 37°C for 6 h. Tube formation was visualized with a camera-equipped inverted Nikon ECLIPSE TS100 microscope.

Computer-assisted morphometric analyses. To quantitatively evaluate vessel density and diameter, LYVE-1-, podoplanin-, and MMRN2-stained cryostat sections were analyzed using a Leica TCS SP2 confocal system. On the acquired images, computer-assisted morphometric analyses were performed using ImageJ software (http://rsb.info.nih.gov).

In vivo lymphatic-vessel function analysis. (i) Lymph drainage analysis. To evaluate the lymph flow of WT and *Emilin1*$^{-/-}$ mice from CD1 and C57BL/6 strains, a modified version of the Miles assay, published by Sugaya et al. (39), was applied. Briefly, a 3% solution of Evans blue dye (Sigma) in PBS was injected (1 μl/g) into the footpads of anesthetized mouse hind limbs. To quantify the lymph flow, draining local and distal lymph nodes were harvested 30 min after injection. The accumulated dye was extracted after the lymph nodes were incubated in formamide (Sigma) overnight at 55°C, and it was quantified spectrophotometrically at 620 nm (GENios Plus; TECAN Italia S.r.L.).

(ii) Lymphatic-vessel leakage assay. To evaluate lymphatic-vessel leakage of WT and *Emilin1*$^{-/-}$ mice, another version of the Miles assay (38), modified by us, was performed. Evans blue dye (3%) was injected (1 μl/g) into the footpads of hind limbs, and after 5 min, an inflammatory agent, mustard oil (Sigma), diluted to 5% in mineral oil (Sigma), was intradermally injected into the ventral skin. As a control, mineral oil only was injected. After 30 min, the animals were sacrificed and the leakage was detected as a blue spot on the underside of the skin. Evans blue was quantified as described above by excising the portion of skin affected by the extravasation and the control skin.

(iii) Intravital lymphangiography. For intravital lymphangiography, 1 μl of a 1% solution of Evans blue dye in PBS was injected intradermally at the inner surface of the rim of the ear. Mouse ear lymphatic vessels were photographed 1, 3, and 5 min after the dye injection.

RNA extraction and RT-PCR. Total cellular RNA was isolated from lymphatic and blood endothelial cells using Trizol (Invitrogen, Milan, Italy) according to the manufacturer's protocol. Reverse transcription (RT) reactions were performed with 1 μg of total RNA using AMV Reverse Transcriptase (Promega Italia, Milan, Italy). RNA was reverse transcribed into first-strand cDNA using

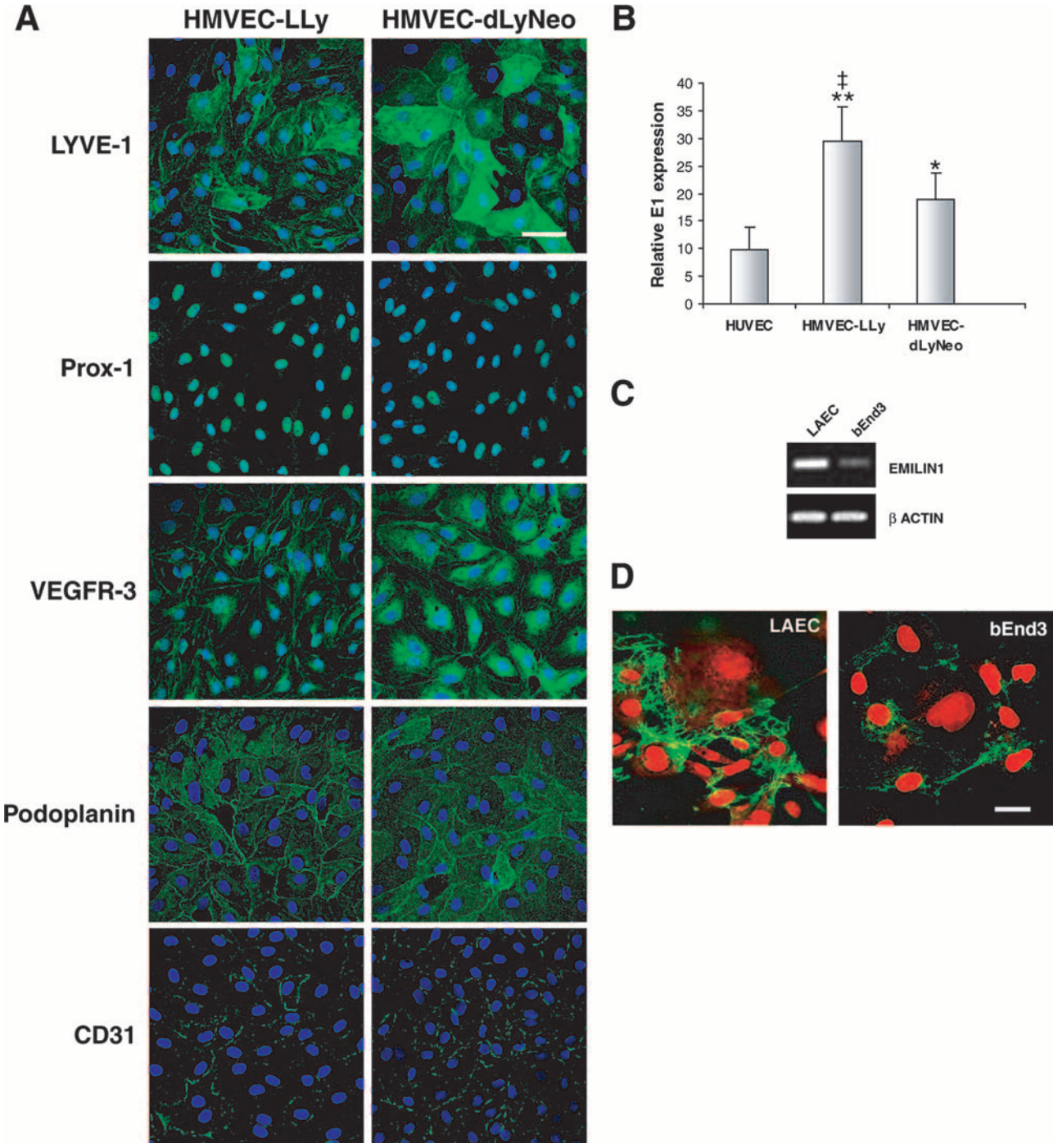

FIG. 1. Human and mouse LECs express high levels of EMILIN1 in vitro. (A) Characterization of human lung and dermal neonatal LECs (HMVEC-LLy and HMVEC-dLyNeo). The positive staining for the lymphatic specific markers, LYVE-1, Prox-1, VEGFR-3, podoplanin, and CD31, is green. Nuclei were stained by ToPro (blue). Scale bar, 45 μm. (B) Quantitative RT-PCR was performed on mRNA extracted from LECs (HMVEC-LLy and HMVEC-dLyNeo, at passage 5) and blood endothelial cells (HUVEC, at passage 4). The relative EMILIN1 (E1) expression versus β-actin was quantified using the SDS 2.1 program. The analysis confirmed abundant EMILIN1 expression by LECs, revealing a threefold increase in HMVEC-LLy (**, $P < 6 \times 10^{-6}$) and a twofold increase in HMVEC-dLyNeo (*, $P < 0.006$) compared with HUVEC. HMVEC-LLy produced higher levels of EMILIN1 then did HMVEC-dLyNeo (‡, $P < 0.006$). (C) Comparative RT-PCR analysis of EMILIN1 mRNA levels in mouse LAECs and in bEnd3 (a mouse endothelioma cell line). (D) Immunofluorescence staining of EMILIN1 (green) shows its abundant production and extracellular deposition by LAECs (left) compared to bEnd3 cells (right). Nuclei were stained red by propidium iodide. Scale bar, 10 μm.

random hexamer primers. The primers for the PCR amplification of mouse EMILIN1 were 5′-TGTGCCTAGGGTAGCATTTTC-3′ and 5′-GAGGCTGAAGAC GCCCAGAG-3′. The size of the amplification product was 320 bp. *Taq* DNA polymerase was obtained from Roche (Monza, Italy). RT-PCR amplification of a 700-bp fragment of β-actin cDNA served as a positive internal control. Amplification products were resolved on 2% agarose gels stained with ethidium bromide.

Quantitative real-time PCR. Real-time PCR was carried out on an ABI PRISM 7900 HT sequence detection system (Applied Biosystems, Warrington, United King-

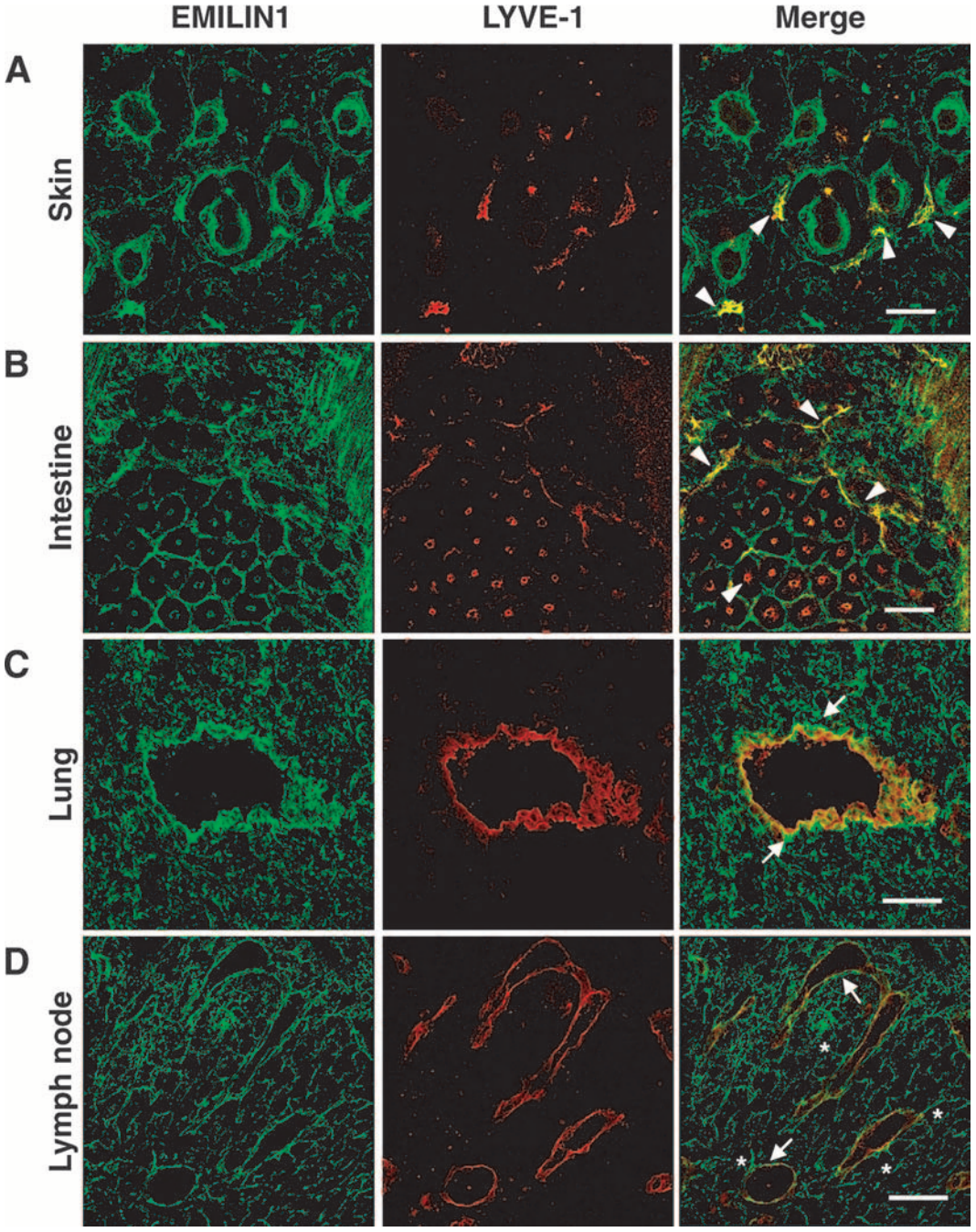

FIG. 2. EMILIN1 is expressed in association with lymphatic vessels. (A to D) Cryostat sections of normal mouse tissues doubly stained with anti-EMILIN1 (green) and anti-LYVE-1 (red) antibodies. In all mouse tissues and organs examined, EMILIN1 was uniformly distributed in the stroma. (A) In the skin, EMILIN1 staining colocalizes with LYVE-1-positive lymphatic vessels surrounding hair follicles (arrowheads; scale bar, 75 μm). (B) In the small intestine, EMILIN1 colocalizes with LYVE-1-positive lacteals and submucosal lymphatic vessels (arrowheads; scale bar, 75 μm). (C and D) At higher magnification, in the lung and lymph nodes, it is more evident that EMILIN1 is distributed at the abluminal surfaces of LECs (arrows; scale bars, 45 μm). In the lymph node, EMILIN1-positive fibers connecting LECs to the surrounding ECM are evident (asterisks).

dom) using the Power Sybr Green PCR Master Mix kit (Applied Biosystems). The calculated amount of EMILIN1 mRNA was normalized to the endogenous reference control mRNA β-actin. All primers were designed with Primer3 software (Universal Probe Library Assay Design Center, Applied Science, Roche, Monza, Italy) and were as follows: for human EMILIN1, 5′ CAGTGTCCCCAAAGCA TCAT 3′ and 5′CACTCCATGTCGGTCACTG T 3′; for human β-actin, 5′ CCA ACCGCGAGAAGATGA 3′ and 5′ CCAGAGGCGTACAGGGATAG 3′. The results were analyzed with SDS 2.1 software (Applied Biosystems).

Statistical analysis. The statistical significance of the results was determined by using the unpaired Student's *t* test. A P value of <0.05 was considered significant.

RESULTS

EMILIN1 is expressed by LECs in vitro. To assess EMILIN1 expression by LECs in vitro, HMVEC-dLyNeo

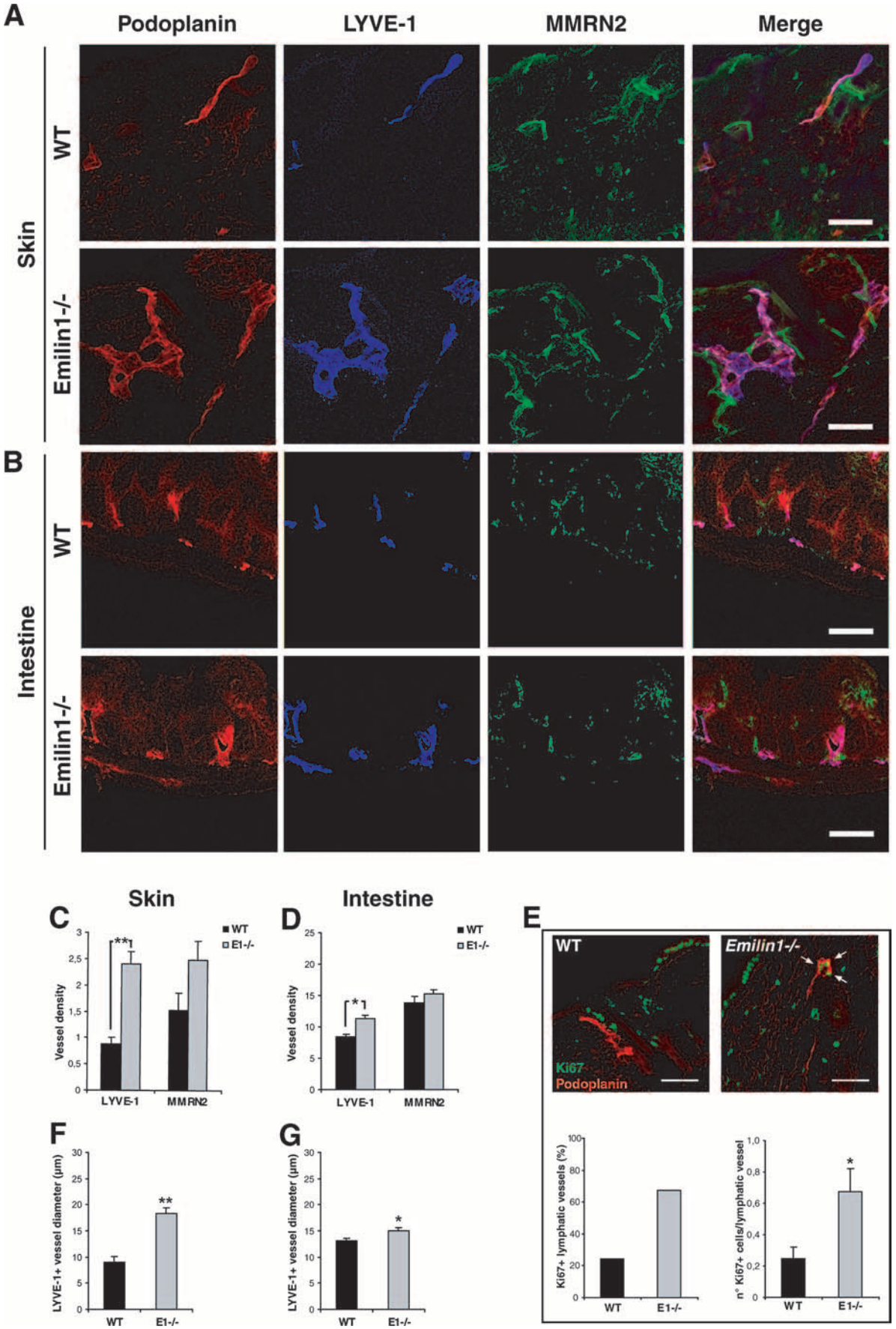
A
Podoplanin
LYVE-1
MMRN2
Merge
Skin
WT
Emilin1-/-
B
Intestine
WT
Emilin1-/-
C
Skin
WT
E1-/-
Vessel density
LYVE-1
MMRN2
D
Intestine
WT
E1-/-
Vessel density
LYVE-1
MMRN2
E
WT
Emilin1-/-
Ki67
Podoplanin
Ki67+ lymphatic vessels (%)
WT
E1-/-
n° Ki67+ cells/lymphatic vessel
WT
E1-/-
F
LYVE-1+ vessel diameter (µm)
WT
E1-/-
G
LYVE-1+ vessel diameter (µm)
WT
E1-/-

and HMVEC-LLy were used. In an immunofluorescence analysis, these cells were strongly positive for the main lymphatic endothelial markers, such as LYVE-1, Prox-1, VEGFR-3, and podoplanin, and weakly positive for CD31 (Fig. 1A). A quantitative RT-PCR analysis performed on mRNA samples from HMVEC-LLy, HMVEC-dLyNeo, and HUVEC demonstrated significantly different EMILIN1 expression by LECs derived from distinct tissues (Fig. 1B). Moreover, this analysis showed, respectively, a threefold and a twofold increase in EMILIN1 mRNA relative levels in HMVEC-LLy and in HMVEC-dLyNeo compared to HUVEC (Fig. 1B). Also, higher EMILIN1 expression was demonstrated by RT-PCR (Fig. 1C) and by immunofluorescence staining (Fig. 1D) in mouse lymphangioma endothelial cells (LAECs) than in mouse blood endothelial cells (bEnd3).

EMILIN1 is expressed in lymphatic vessels. To directly investigate the role of EMILIN1 in vivo, we first determined EMILIN1 expression in relationship with lymphatic vessels. In mouse skin, intestine, lung, and lymph node, EMILIN1 was closely associated with lymphatic vessels and colocalized with the LEC-specific marker LYVE-1 (Fig. 2). In detail, EMILIN1 was weakly expressed in the skin stroma, while an intense staining was observed in the connective tissue layer surrounding hair follicles, particularly in colocalization with LYVE-1-positive lymphatic vessels (Fig. 2A). EMILIN1 staining was more intense in the intestine smooth muscle layer, and it was superimposable with lacteals and submucosal lymphatic vessels (Fig. 2B). Finally, EMILIN1 was abundantly expressed in the lung and lymph node tissue stroma. At higher magnification, EMILIN1 was clearly expressed at the abluminal surfaces of LECs (Fig. 2C), and EMILIN1-positive fibers radiating from LECs to the surrounding perivascular area were frequently detected (Fig. 2D).

Hyperplastic and enlarged lymphatic vessels in *Emilin1*-deficient mice. The expression of EMILIN1 in close association with lymphatic vessels prompted us to analyze *Emilin1*-deficient mice in order to investigate if lack of EMILIN1 induced any abnormality of the lymphatic vasculature. For this purpose, we examined both *Emilin1*-deficient CD1 and C57BL/6 mice, and the results obtained were similar. To assess the growth and the patterning of lymphatic vasculature, an immunofluorescence analysis was performed with anti-LYVE-1 and anti-podoplanin antibodies to detect lymphatic vessels and anti-MMRN2 antibodies to detect blood vessels. We observed not only that the lymphatic vessels were more abundant in *Emilin1*$^{-/-}$ mice, but also that compared to those of WT mice, the lymphatic vessels were more dilated in the skin (Fig. 3A), as well as in the intestine (Fig. 3B). A quantitative analysis confirmed that the number of LYVE-1-positive vessels was significantly higher in *Emilin1*$^{-/-}$ mouse tissues (Fig. 3C and D), whereas the number of MMNR2-positive blood vessels was not significantly increased. Accordingly, a double-immunofluorescence analysis for the proliferation marker Ki67 and for podoplanin revealed numerous proliferating LECs in *Emilin1*$^{-/-}$ mice (Fig. 3E, top right). In detail, more than 67% of the lymphatic vessels observed in the skin of *Emilin1*$^{-/-}$ mice presented Ki67-positive LECs, a percentage that almost reached 24% in WT mice (Fig. 3E, bottom left). The average number of Ki67-positive cells per lymphatic vessel was significantly higher ($P = 0.015$) in *Emilin1*$^{-/-}$ mice than in their WT littermates. A computer-assisted morphometric analysis confirmed that the diameters of lymphatic vessels were also significantly increased in the skin (Fig. 3F) and in the intestine (Fig. 3G) in *Emilin1*$^{-/-}$ mice.

In addition, *Emilin1*$^{-/-}$ mouse lymph nodes showed a significant increase ($P < 2 \times 10^{-6}$) in lymphatic-vessel, but not in blood vessel, density (Fig. 4A and B) by a computer-assisted morphometric analysis. Also, the diameters of lymphatic vessels in *Emilin1*$^{-/-}$ mouse lymph nodes were greater (Fig. 4C), and the difference from WT vessels was confirmed by ImageJ software analysis to be highly significant ($P < 2 \times 10^{-7}$) (Fig. 4D).

The abnormal architecture of lymphatic vessels in *Emilin1*$^{-/-}$ mice was even more evident when we immunostained whole-mount preparations from the ear skin with LYVE-1. Lymphatic vessels of *Emilin1*$^{-/-}$ mice presented a tortuous and irregular pattern and frequently displayed buds (Fig. 5A, right). In the intestine of WT mice, LYVE-1-positive submucosal lymphatic vessels were generally well organized and presented a regular lumen (Fig. 5B, left). In contrast, lymphatic vessels in *Emilin1*$^{-/-}$ mice formed a dense network and were frequently irregular and dilated (Fig. 5B, right). Dysmorphic structures were also detected in subserosal lymphatic vessels, and wide lacunae were occasionally present (Fig. 5C and D, right). Similar structures were not detected in intestinal lymphatic vessels of WT mice (Fig. 5C and D, left).

***Emilin1*-deficient mice develop larger lymphangiomas.** To evaluate the influence of EMILIN1 in lymphatic-vessel growth in vivo, a model of neolymphangiogenesis was investigated by inducing the formation of hyperplastic lymphatic vessels. After

FIG. 3. Hyperplasia and enlarged lymphatic vessels in *Emilin1*-deficient mice. (A and B) Immunofluorescence staining of mouse skin (A) and small intestine (B) for podoplanin (red), LYVE-1 (blue), and MMRN2 (green) revealed a higher number of enlarged lymphatic vessels in the skin (A, bottom) and in the intestines (B, bottom) of *Emilin1*$^{-/-}$ mice ($n = 10$) than in their WT littermates ($n = 10$) (A and B, top). (C and D) Vessel counts per field. In a double-blind study, transversally oriented cryostat sections were observed at ×40 magnification, and the vessel density was evaluated in random fields. The number (mean ± standard error [SE]) of LYVE-1-positive vessels was significantly increased in the skin (C) (**, $P < 1.5 \times 10^{-7}$) and in the intestine (D) (*, $P < 0.0002$) of *Emilin1*$^{-/-}$ mice. The numbers (mean ± SE) of MMRN2-positive blood vessels were not significantly different in the two mouse genotypes. (E) Immunofluorescence analysis of mouse skin for the proliferation marker Ki67 (green) and for podoplanin (red) showed a higher number of proliferating LECs in *Emilin1*$^{-/-}$ ($n = 5$) than in WT ($n = 5$) mice. Representative images are shown above the graphs; the arrows indicate Ki67-positive LECs. The count of Ki67-positive cells per lymphatic vessel in mouse skin cryostat sections revealed a threefold-higher percentage of Ki67-positive lymphatic vessels (bottom left) and a significant increase in Ki67-positive cells per lymphatic vessel (bottom right) (mean ± SE; *, $P = 0.015$) in *Emilin1*$^{-/-}$ mice compared to their WT littermates. Ki67 quantification analysis was performed, examining 49 WT and 55 *Emilin1*$^{-/-}$ mouse lymphatic vessels. (F and G) A computer-assisted image analysis (ImageJ software) confirmed that the diameters (mean ± SE) of lymphatic vessels were significantly increased in the skin (F) (**, $P < 6 \times 10^{-6}$) and in the intestine (G) (*, $P = 0.03$) of *Emilin1*$^{-/-}$ mice. E1, EMILIN1. Scale bars, 75 μm.

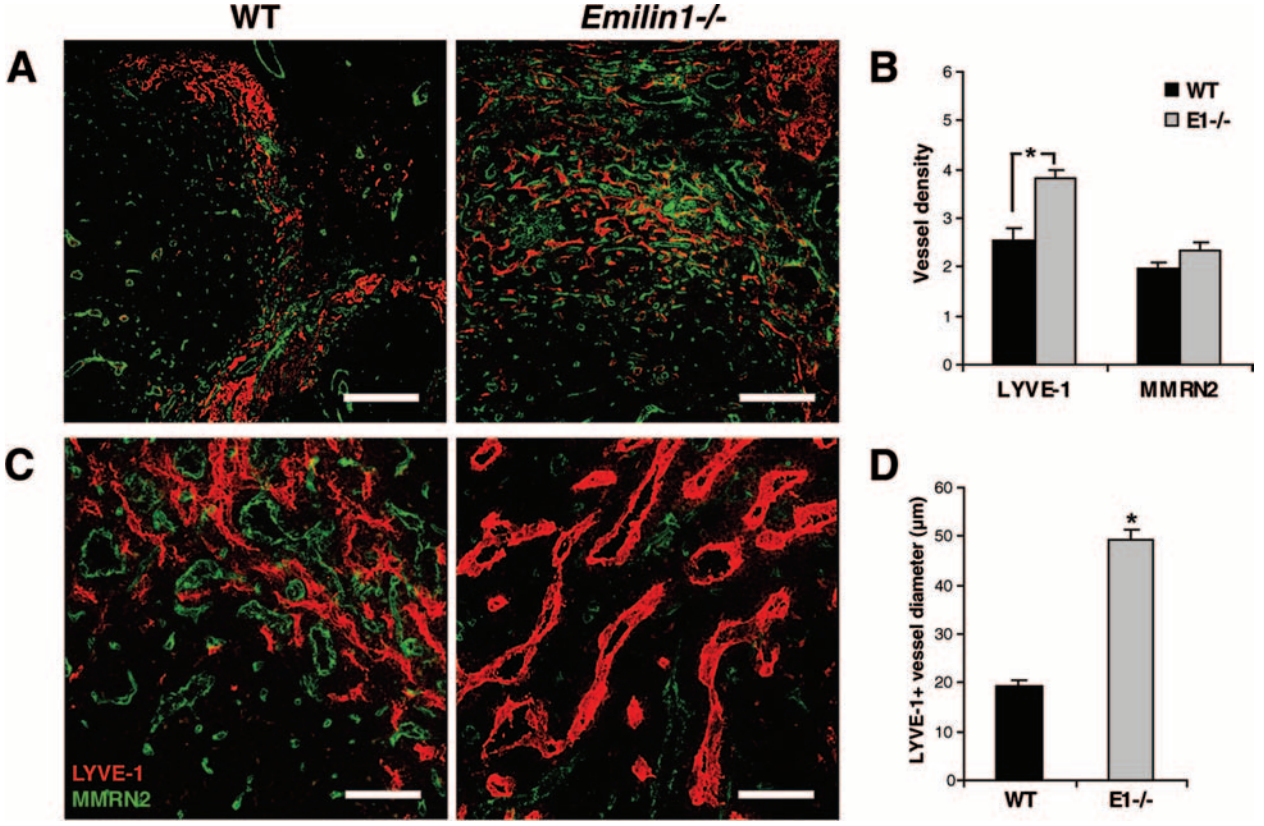

FIG. 4. Hyperplasia and enlarged lymphatic vessels in lymph nodes of *Emilin1*-deficient mice. (A) Representative immunofluorescence images of mouse inguinal lymph node cryostat sections stained for LYVE-1 (red) and MMRN2 (green). Scale bars, 300 μm. (B) ImageJ software analysis revealed that the relative area occupied by lymphatic vessels in lymph nodes of *Emilin1*$^{-/-}$ (E1−/−; $n = 9$) mice was significantly higher (mean ± standard error [SE]; *, $P < 2 \times 10^{-6}$) than in those of their WT littermates ($n = 9$). (C) Higher-magnification images show dilated LYVE-1-positive vessels (right). Scale bars, 75 μm. (D) The mean value ± SE of the diameters (ImageJ software analysis) of lymphatic vessels is reported. *, $P < 2 \times 10^{-7}$.

treatment with Freund's incomplete adjuvant, mice developed benign tumors (lymphangiomas) that appeared as clearly delimited white solid plaques localized on the liver and diaphragm surfaces. *Emilin1*$^{-/-}$ ($n = 18$) and *Emilin1*$^{+/-}$ ($n = 9$) mice developed more numerous and larger plaques than their WT littermates ($n = 18$). In Fig. 6A, images representing typical lymphangioma growth in WT, *Emilin1*$^{+/-}$, and *Emilin1*$^{-/-}$ mice are shown. To better quantify the phenomena observed, each mouse was assigned to one of three lymphangioma development classes, considering both the number and the size of the plaques: class I corresponded to few ($n < 3$) and small (diameter, <2 mm) lymphangioma plaques, class III to numerous ($n > 7$) and large (diameter, >4 mm) plaques, and class II to an intermediate situation. Most of *Emilin1*$^{-/-}$ lymphangiomas (72.2%) belonged to class III (Fig. 6B).

In accord with the high level of EMILIN1 expression by LAECs (Fig. 1), WT mouse lymphangiomas were also highly positive, and staining for EMILIN1 was strictly associated with LYVE-1-positive lymphatic vessels (data not shown). To investigate if the different sizes of lymphangiomas were linked to lymphatic vascularization, we performed an immunofluorescence analysis for LYVE-1 and MMNR2 expression. The lymphatic-vessel density was qualitatively evaluated in double-blind tests as low, medium, and high class, and the results are shown in Fig. 6C. Sixty percent of *Emilin1*$^{-/-}$ lymphangiomas fell in the high class, while no lymphangiomas induced in WT mice belonged to that class. On the contrary, 66.7% of WT lymphangiomas were classified in the low class, and *Emilin1*$^{+/-}$ lymphangiomas had intermediate values. A quantitative analysis performed with ImageJ software confirmed that the number of LYVE-1-positive vessels was significantly higher in heterozygous mice (Fig. 6D) ($P < 0.04$) and even more highly significant in *Emilin1*-deficient mice ($P < 6 \times 10^{-5}$). No differences were observed for MMRN2-positive blood vessels (Fig. 6D). Some representative images of lymphangioma vessel density are shown in Fig. 6E. In addition, whole-mount staining showed that lymphatic vessels of *Emilin1*$^{-/-}$ lymphangiomas displayed a more intricate network of tortuous lymphatic vessels with irregular lumen than in WT mice (Fig. 6F). Altogether, these results support the notion that the absence of EMILIN1 induces unregulated and abnormal growth of lymphatic vessels. To demonstrate this assertion, LECs from lymphangiomas induced in WT and *Emilin1*$^{-/-}$ mice were isolated and proliferation and tube formation assays were performed. *Emilin1*$^{-/-}$ LAECs, when grown on cover glass slips, presented a significant increase in Ki67-positive cell numbers ($P < 0.006$) (Fig. 6G), indicating a higher proliferation rate. WT LAECs efficiently formed a network of tube-like structures

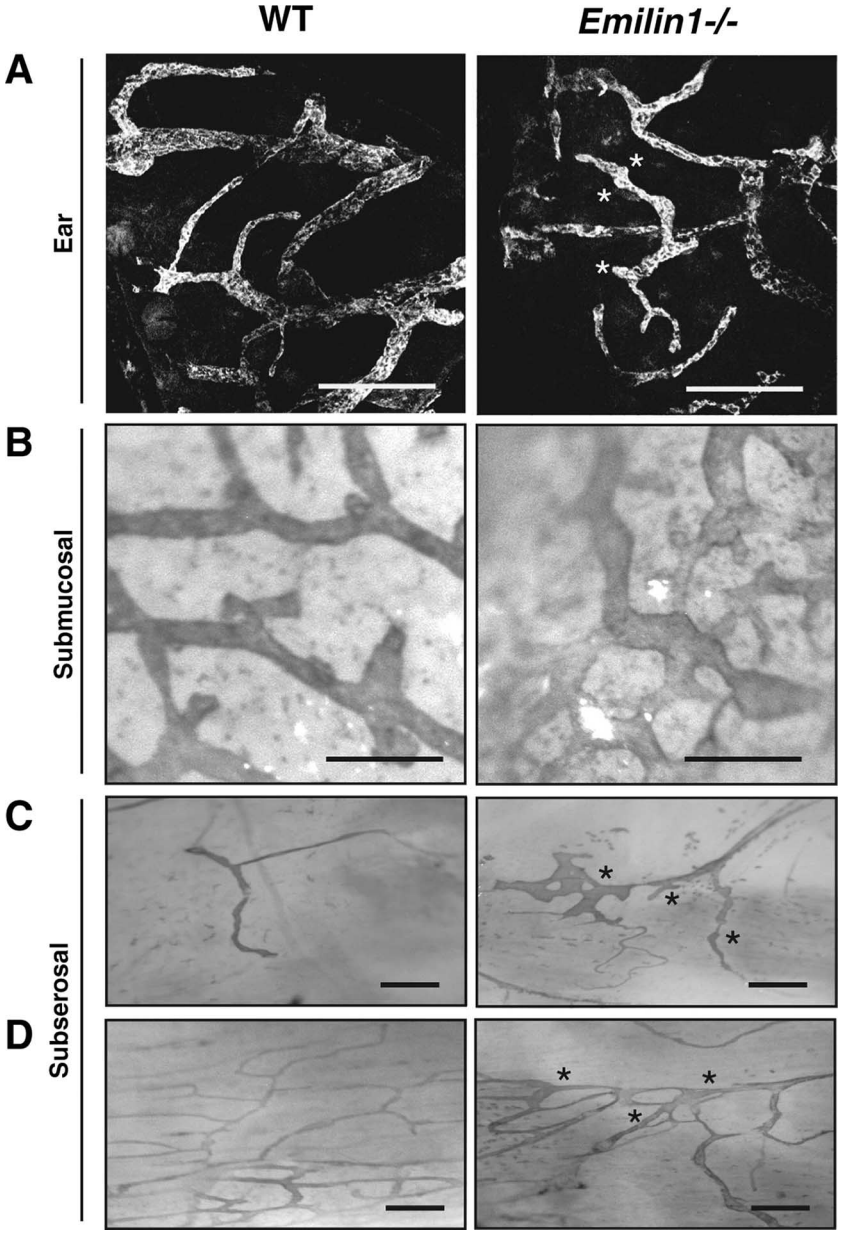

FIG. 5. Abnormal lymphatic-vessel morphology in *Emilin1*-deficient mice. (A) Whole-mount immunofluorescence staining with LYVE-1 shows an irregular morphology of ear lymphatic vessels. The white asterisks indicate buds on lymphatic vessels. Scale bars, 300 μm. (B to D) LYVE-1 diaminobenzidine-peroxidase whole-mount staining of submucosal (B) (scale bars, 500 μm) and subserosal (C and D) (scale bars, 500 μm) lymphatic vessels. The black asterisks indicate dysmorphic structures.

when seeded onto Matrigel-coated dishes (Fig. 6H, left). On the other hand, *Emilin1*$^{-/-}$ LAECs demonstrated a lesser capability; the resulting tube-like structures were poorly organized (Fig. 6H, right) compared to those of WT cells.

***Emilin1* deficiency affects LEC anchorage.** To investigate the lymphatic defects caused by *Emilin1* deficiency at the ultrastructural level, transmission electron microscopy analysis was performed on WT and *Emilin1*$^{-/-}$ mouse skin specimens. WT lymphatics of skin displayed an irregular lumen with frequent abluminal endothelial cell projections into the ECM. The abluminal plasma membranes of the endothelial cells showed a discontinuous basal lamina and bundles of microfibrils, i.e., the anchoring filaments. These radiated from the membranes of LECs and reached small elastin fibrils (with diameters ranging from 150 to 500 nm) (Fig. 7A); in the connection region, the LEC membrane appeared to be modified and the subcortical associated cytoskeleton was characterized by the presence of thin filaments (Fig. 7A, inset). *Emilin1*$^{-/-}$ lymphatic vessels showed differences concerning the abluminal surfaces of the endothelial cells: rare endothelial cell projections into the ECM were detected, giving a smooth appearance to the abluminal surface, and the number of bundles of anchoring filaments was significantly reduced with respect to the WT (Fig. 7B and C) ($P < 0.005$). Another frequent finding was the

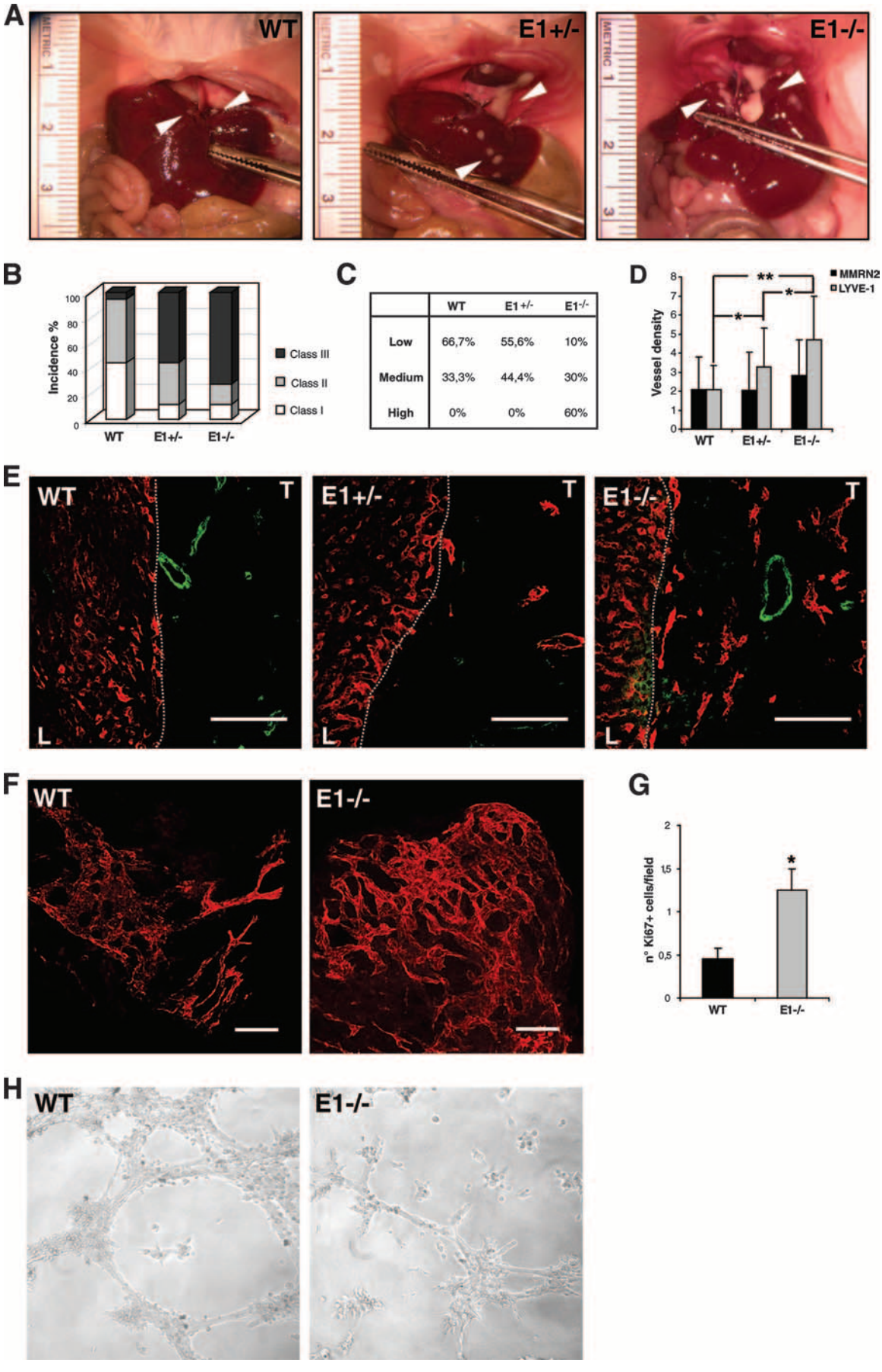
A
WT
E1+/-
E1-/-
B
Incidence %
100
80
60
40
20
0
WT
E1+/-
E1-/-
Class III
Class II
Class I
C
WT
E1+/-
E1-/-
Low
66,7%
55,6%
10%
Medium
33,3%
44,4%
30%
High
0%
0%
60%
D
MMRN2
LYVE-1
Vessel density
**
*
*
WT
E1+/-
E1-/-
E
WT
T
L
E1+/-
T
L
E1-/-
T
L
F
WT
E1-/-
G
n° Ki67+ cells/field
2
1,5
1
0,5
0
*
WT
E1-/-
H
WT
E1-/-

presence of abnormal intercellular junctions. WT LECs showed characteristic overlapping junctions (Fig. 7D), whereas *Emilin1*$^{-/-}$ LECs frequently presented multiple overlapping contacts. These junctions did not originate from an interdigitation but were the result of an extended overlap among several LECs that appeared thin and tightly packed and developed adherens junctions (Fig. 7E). These aspects were never detected in WT animals.

Impaired lymphatic-vessel function in *Emilin1*-deficient mice. Several approaches were pursued to understand if the lymphatic vessel abnormalities detected in *Emilin1*$^{-/-}$ mice might be functionally relevant. WT ($n = 8$) and *Emilin1*$^{-/-}$ ($n = 8$) mice were intradermally injected with Evans blue dye in the hind limb footpads, and then their lymphatic drainage was evaluated. The lymphatic vessels of *Emilin1*$^{-/-}$ mice were less able to take up and transport lymph than those of their WT littermates: after 30 min, gross examination of the distal lymph nodes of WT mice showed an intense blue staining (Fig. 8A); on the other hand, the lymph nodes of *Emilin1*$^{-/-}$ mice appeared weakly colored and marked only by a blue halo. Thus, WT lymph nodes contained significantly greater amounts of dye than those of *Emilin1*$^{-/-}$ mice (Fig. 8B) ($P < 1.5 \times 10^{-6}$), suggesting that *Emilin1* deficiency induces inefficient lymph drainage.

To further investigate these findings using a second, independent method, we monitored lymph leakage under normal conditions and in response to mustard oil, an inflammatory agent (Fig. 8C). The dye extravasation was detected as a blue spot on the underside of the skin 30 min after injection of Evans blue dye into the footpads of WT ($n = 7$) and *Emilin1*$^{-/-}$ ($n = 7$) mice and the application of mustard oil. The size of this spot and the intensity of its staining were always increased in *Emilin1*$^{-/-}$ mice compared with their WT littermates (Fig. 8C), suggesting greater lymph leakage. A quantitative analysis of the dye content confirmed that lymph leakage was enhanced in *Emilin1*$^{-/-}$ mice compared with their WT littermates (Fig. 8D). Baseline leakage was significantly higher in *Emilin1*$^{-/-}$ mice compared with that of their WT littermates ($P < 6 \times 10^{-5}$). Mustard oil treatment increased the leakage in WT mice to a greater extent, and the difference between the two mouse genotypes was less evident but still statistically significant (Fig. 8D) ($P < 0.0085$).

Next, intravital lymphangiography 1 min after Evans blue dye injection demonstrated that markedly leaky lymphatic vessels were already visualized in *Emilin1*$^{-/-}$ ($n = 5$) mouse ears (Fig. 8E, bottom), especially near the site of injection. After 3 and 5 min, the extent of leakage progressively increased in *Emilin1*$^{-/-}$ mouse skin, and also, the more distal lymphatic vessels presented signs of dye extravasation (Fig. 8E, bottom). On the other hand, leakage was never observed in WT ($n = 5$) mice (Fig. 8E, top). Of note, the irregular and tortuous pattern of *Emilin1*$^{-/-}$ mouse lymphatic vessels compared with those of their WT littermates (Fig. 8E, processed images [right]). In accord with lymphatic-vessel defects, *Emilin1*$^{-/-}$ mice showed swelling of the paws, indicating mild lymphedema (Fig. 8F), whereas the formation of ascites was never observed in *Emilin1*-deficient mice.

DISCUSSION

The role played by ECM, in which lymphatics are embedded, is considered important for lymphatic function (40); however, its composition and architecture have seldom been taken into consideration when the biology and the pathology of the lymphatic system have been studied. In the quest to identify new lymphatic molecular players, we report for the first time an abnormal lymphatic phenotype in *Emilin1*-deficient mice and demonstrate the involvement of EMILIN1 in the structure and function of lymphatic vessels, as well as in lymphangiogenesis.

The present study extended, by quantitative RT-PCR, previous microarray data showing that LECs express abundant EMILIN1 mRNA (33). We detected a twofold and a threefold increase of EMILIN1 mRNA relative levels, compared to HUVEC, in human dermal neonatal and lung microvascular LECs, respectively. This difference is in agreement with the phenotypic heterogeneity of LECs isolated from different organs and different segments of the lymphatic vasculature, as previously reported (17). Moreover, RT-PCR and immunofluorescence analyses showed much higher EMILIN1 production and deposition in mouse lymphatic cells than in blood endothelial cells of mouse origin. Consistent with the absence of a basement membrane in vivo, LECs secrete very little ECM in comparison to blood endothelial cells (15); thus, the abundant EMILIN1 production in vitro suggested a potential involvement of this protein in the structure and function of lymphatic vessels.

EMILIN1 was expressed in all mouse tissues in association with lymphatic vessels, and it frequently colocalized with the abluminal surfaces of LECs. Moreover, EMILIN1-positive fi-

FIG. 6. Lymphangioma induction in *Emilin1*-deficient mice. (A) Representative images show that lymphangioma plaques were more numerous and larger in *Emilin1*$^{-/-}$ mice (the arrowheads indicate the white plaques that developed on the liver and diaphragm surfaces). (B) Lymphangioma development. Class I corresponds to few and small lymphangioma plaques, class III to numerous and large plaques, and class II to an intermediate situation. (C) Lymphatic-vessel density. Lymphangioma cryostat sections were stained with LYVE-1, and in a double-blind study, lymphatic-vessel densities were evaluated as low, medium, and high. (D) Quantitative ImageJ analysis. The average fluorescence intensity confirmed that lymphatic-vessel density was significantly increased in *Emilin1*$^{-/-}$ (E1−/−) and *Emilin1*$^{+/-}$ (E1+/−) mouse lymphangiomas compared with those of their WT littermates (*, $P < 0{,}04$; **, $P < 6 \times 10^{-5}$). No significant differences were observed for MMRN2-positive blood vessels. The error bars indicate standard deviations. (E) Immunofluorescence analysis of cryostat sections of mouse lymphangiomas. LYVE-1-positive lymphatic vessels (red; note that liver sinusoids are also positive) and MMRN2-positive blood vessels (green). L, liver; T, tumor. Scale bars, 75 μm. (F) Whole mounts of diaphragm plaques of WT and *Emilin1*$^{-/-}$ mice stained with LYVE-1. Scale bars, 300 μm. (G) Proliferation rate. WT and *Emilin1*$^{-/-}$ LECs isolated from mouse lymphangiomas (LAECs) were seeded onto glass coverslips and grown in EBM plus 2% fetal bovine serum. After 72 h, Ki67-positive nuclei per field were counted at ×60 magnification. *, $P < 0.006$. (H) Tube formation assay. WT and *Emilin1*$^{-/-}$ LAECs were seeded onto Matrigel and allowed to form tube-like structures for 6 h. The images were acquired with a camera-equipped inverted microscope (×10 original magnification).

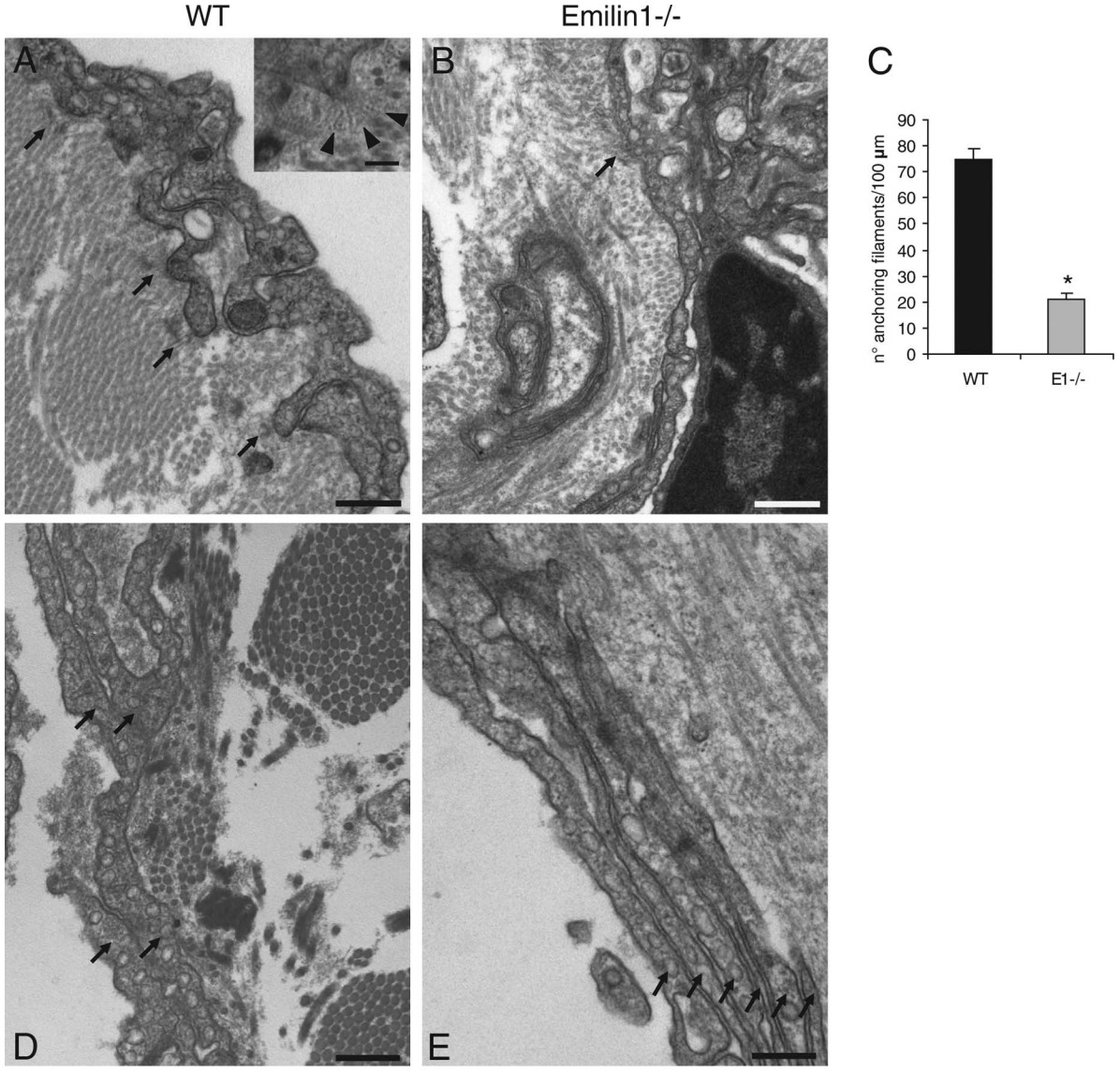

FIG. 7. EMILIN1 deficiency affects LEC anchorage. Transmission electron microscopy analysis of WT (A and D) and *Emilin1*$^{-/-}$ (B and E) skin lymphatic vessels. (A) WT LECs display characteristic bundles of anchoring filaments (arrows), which extend from the abluminal side of the plasma membrane into the adjoining connective tissue (inset, arrowheads). (B) *Emilin1*$^{-/-}$ LECs show reduced numbers of tufts of anchoring filaments (arrow). (C) Quantitative analysis of the bundles of anchoring filaments in WT and *Emilin1*$^{-/-}$ skin lymphatics ($n = 10$). The values express means ± standard deviations per 100 μm and show a significant reduction in the number of *Emilin1*$^{-/-}$ lymphatic vessels ($P < 0.005$). (D) Normal lymphatic endothelium showing typical overlapping junctions (arrows) between adjacent LECs. (E) Abnormal overlapping junctions in an *Emilin1*$^{-/-}$ lymphatic vessel involving several LECs (arrows); the LECs in these areas appeared thin and packed and developed adherens junctions. Scale bar, 200 nm; inset scale bar, 60 nm.

bers were observed radiating from LECs to the surrounding ECM. Considering the association of EMILIN1 with elastic fibers, its expression in the lymphatic perivascular area indicates that EMILIN1 represents a component of the lymphatic fibrillar elastic apparatus previously described (18). This apparatus is formed by three hierarchical components disposed concentrically around lymphatic capillaries: the oxytalan fibers, identified as fibrillin microfibrils (35), connected directly to LECs and representing the real anchoring filaments; then elaunin fibers; and, more distant from the vessel, elastic fibers (18). It has been postulated that this apparatus is highly sensitive to interstitial stresses. An increase in the interstitial fluid volume exerts tension on LECs, widening the capillary lumen and opening the overlapping cell junctions, thus facilitating lymph formation (40). EMILIN1 involvement in this delicate physiologic mechanism was demonstrated by a comparative study between WT and *Emilin1*$^{-/-}$ mice that highlighted the fact that *Emilin1* deficiency induces defects in lymphatic vascular structure and function. *Emilin1*$^{-/-}$ mice display hyperplasia and enlargement of dermal, as well as visceral, lymphatic vessels, and frequently these vessels present a tortuous and irregular pattern. Moreover, LECs of *Emilin1*$^{-/-}$ mice showed in an ultrastructural examination a significant reduction in the number of anchoring filaments and abnormal multiple over-

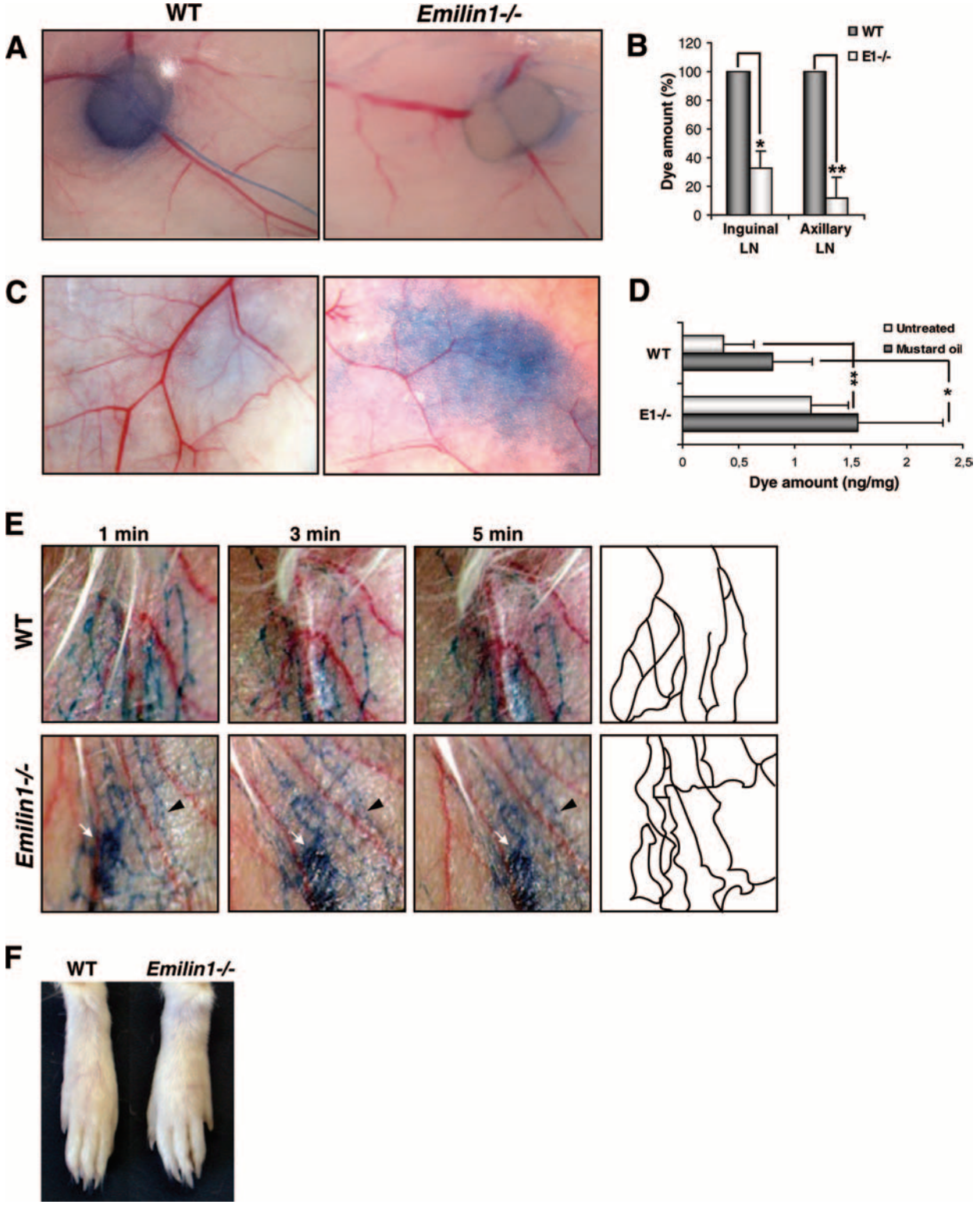

FIG. 8. Impaired lymphatic function in *Emilin1*-deficient mice. (A) Evans blue dye accumulation in inguinal lymph nodes 30 min after dermal injection into the footpad; the dye is barely detectable in *Emilin1*$^{-/-}$ mice (right), whereas the inguinal lymph node is easily visualized in WT mice (left). The images were acquired with a camera-equipped dissection microscope. (B) Evans blue dye contents (mean ± standard deviation [SD]) in inguinal and axillary lymph nodes expressed as percentages of the amount (ng/mg) of dye in WT lymph nodes after dermal injection into the footpad (*, $P < 1.5 \times 10^{-6}$; **, $P < 8 \times 10^{-7}$). E1−/−, *Emilin1*$^{-/-}$. (C) Lymph leakage. Spots of Evans blue extravasation in mustard oil-treated mouse skin. (D) Quantification (mean ± SD) of Evans blue dye content in treated (*, $P < 0.0085$) and untreated (**, $P < 6 \times 10^{-5}$) skin. (E) Intravital lymphangiography. To visualize lymphatic vessels, 2 μl of 1% Evans blue dye was intradermally injected into the rims of the ears of WT ($n = 5$) and *Emilin1*$^{-/-}$ ($n = 5$) mice. At 1, 3, and 5 min, the ears were photographed with a camera-equipped dissection microscope. One representative experiment is shown. The arrows indicate the major leakage areas in *Emilin1*$^{-/-}$ mouse ears; the arrowheads indicate the extension of the leakage (bottom). (Right) The irregular morphology of *Emilin1*$^{-/-}$ mouse lymphatic vessels is evidenced by processed images. (F) Peripheral edema. Hind limbs of WT and *Emilin1*$^{-/-}$ mice of equal weight were compared.

lapping intercellular junctions. Lymphatic-vessel defects were associated in *Emilin1*$^{-/-}$ mice with impaired lymph drainage, enhanced lymph leakage, and mild lymphedema. These findings indicate that the absence of EMILIN1 causes defective ECM anchorage of LECs and, consequently, dilation of the lymphatic-vessel lumen and reduced responsiveness to interstitial pressure variations. The resulting abnormal lymphatic function is more likely the consequence of enhanced lymph leakage than of defective lymph transport by collecting lymphatic vessels. In this view, the main phenotype characteristic of *Emilin1* null mice is in lymph formation. Notably, the phenotype displayed by *Emilin1*$^{-/-}$ mice is the first abnormal lymphatic phenotype associated with deficiency of an ECM protein, and thus, it represents a useful tool to demonstrate the supposed fundamental role of anchoring filaments and the lymphatic perivascular elastic apparatus, as well as of the surrounding ECM, in lymphatic-vessel function.

In contrast to other recently described lymphatic-lineage gene-targeting mouse models that in most cases are embryonic or perinatal lethal (reviewed in reference 41), homozygous disruption of the *Emilin1* gene induces a mild phenotype, indicating that the protein does not play a key role in the developmental processes of the lymphatic vasculature. On the contrary, it seems to be involved in regulation of the growth of lymphatic vessels and in maintenance of their integrity, a fundamental requirement for an efficient lymphatic-system function. Malfunctions of the lymphatic system rarely result in human life-threatening diseases. The most common disorder is lymphedema, which derives from the failure of lymph transport (23). Lymphedema may be an inherited disease caused by mutations identified in genes encoding VEGFR-3 (45), FOXC2 (14, 16), and Sox18 (20) or it may be acquired and occur after obstruction or damage of lymphatic vessels (23). Considering the lymphatic phenotype displayed by *Emilin1*$^{-/-}$ mice, we suppose that *Emilin1* deficiency may resemble early stages of acquired lymphedema. Tissue inflammation following injury, exposure to radiation, or infection may induce the release of proteolytic enzymes that degrade EMILIN1 and render lymphatic vessels nonresponsive to the changes in the interstitium and therefore may cause an acute lymphatic insufficiency. This hypothesis is supported by preliminary unpublished data about EMILIN1-specific degradation by several enzymes abundantly present in the inflammation microenvironment. Moreover, Negrini and colleagues have recently demonstrated that fragmentation and disorganization of ECM components in the lung lead to interstitial and eventually severe edema (29).

Finally, the observations that *Emilin1*$^{-/-}$ mice display lymphatic hyperplasia and develop larger lymphangiomas associated with an increased lymphatic vessel density than their WT littermates suggest a complementary role of EMILIN1 in this context as a lymphangiogenesis modulator. This hypothesis is supported by the finding that threefold more Ki67-positive nuclei colocalizing with podoplanin-positive LECs were found in samples obtained from *Emilin1*$^{-/-}$ mice than in those from WT mice. Thus, EMILIN1 may play for LECs a regulator function similar to that of thrombospondins (TSPs) for blood endothelial cells: both TSP-1 and TSP-2 were reported to inhibit angiogenesis in vivo, contributing to the normal quiescence of blood vasculature (2, 21, 42, 43). Alternatively, the increased lymphatic-vessel density of *Emilin1*$^{-/-}$ mice may be a consequence of the higher levels of the active form of TGF-β1, since pro-TGF-β1 maturation is not adequately regulated by the absence of EMILIN1 in these mice (47). This growth factor may promote lymphangiogenesis directly, since LECs express high levels of the TGF-β1 coreceptor endoglin (31), or indirectly as a VEGF-C inducer (13). Further studies will be necessary to unveil the precise underlying molecular mechanisms.

In conclusion, the present study identifies EMILIN1 as an important component of the lymphatic perivascular elastic apparatus and demonstrates its involvement in the structure-function relationship of lymphatic vessels, as well as in lymphangiogenesis. Notably, this is the first abnormal lymphatic phenotype associated with the deficiency of an ECM protein, and we suggest that it represents a novel model of lymphatic dysfunction.

ACKNOWLEDGMENTS

This work was supported by the Associazione Italiana per la Ricerca sul Cancro and by department grants to A. C. and by the Fondo per gli Investimenti della Ricerca di Base (RBAU017F3F) to G.M.B.

We thank Maria Teresa Mucignat for technical assistance.

REFERENCES

1. **Banerji, S., J. Ni, S. X. Wang, S. Clasper, J. Su, R. Tammi, M. Jones, and D. G. Jackson.** 1999. LYVE-1, a new homologue of the CD44 glycoprotein, is a lymph-specific receptor for hyaluronan. J. Cell Biol. **144:**789–801.
2. **Bornstein, P., L. C. Armstrong, K. D. Hankenson, T. R. Kyriakides, and Z. Yang.** 2000. Thrombospondin 2, a matricellular protein with diverse functions. Matrix Biol. **19:**557–568.
3. **Breiteneder-Geleff, S., A. Soleiman, H. Kowalski, R. Horvat, G. Amann, E. Kriehuber, K. Diem, W. Weninger, E. Tschachler, K. Alitalo, and D. Kerjaschki.** 1999. Angiosarcomas express mixed endothelial phenotypes of blood and lymphatic capillaries: podoplanin as a specific marker for lymphatic endothelium. Am. J. Pathol. **154:**385–394.
4. **Bressan, G. M., D. Daga-Gordini, A. Colombatti, I. Castellani, and D. Volpin.** 1993. Emilin, a component of elastic fibers preferentially located at the elastin-microfibrils interface. J. Cell Biol. **121:**201–212.
5. **Christian, S., H. Ahorn, M. Novatchkova, P. Garin-Chesa, J. E. Park, G. Weber, F. Eisenhaber, W. J. Rettig, and M. C. Lenter.** 2001. Molecular cloning and characterization of EndoGlyx-1, an EMILIN-like multisubunit glycoprotein of vascular endothelium. J. Biol. Chem. **276:**48588–48595.
6. **Colombatti, A., G. M. Bressan, I. Castellani, and D. Volpin.** 1985. Glycoprotein 115, a glycoprotein isolated from chick blood vessels, is widely distributed in connective tissue. J. Cell Biol. **100:**18–26.
7. **Colombatti, A., R. Doliana, S. Bot, A. Canton, M. Mongiat, G. Mungiguerra, S. Paron-Cilli, and P. Spessotto.** 2000. The EMILIN protein family. Matrix Biol. **19:**289–301.
8. **Cueni, L. N., and M. Detmar.** 2006. New insights into the molecular control of the lymphatic vascular system and its role in disease. J. Investig. Dermatol. **126:**2167–2177.
9. **De Cock, H. E., V. K. Affolter, T. B. Farver, L. Van Brantegem, B. Scheuch, and G. L. Ferraro.** 2006. Measurement of skin desmosine as an indicator of altered cutaneous elastin in draft horses with chronic progressive lymphedema. Lymphat. Res. Biol. **4:**67–72.
10. **Doliana, R., M. Mongiat, F. Bucciotti, E. Giacomello, R. Deutzmann, D. Volpin, G. M. Bressan, and A. Colombatti.** 1999. EMILIN, a component of the elastic fiber and a new member of the C1q/tumor necrosis factor superfamily of proteins. J. Biol. Chem. **274:**16773–16781.
11. **Doliana, R., S. Bot, P. Bonaldo, and A. Colombatti.** 2000. EMI, a novel cysteine-rich domain of EMILINs and other extracellular proteins, interacts with the gC1q domains and participates in multimerization. FEBS Lett. **484:**164–168.
12. **Ebata, N., Y. Nodasaka, Y. Sawa, Y. Yamaoka, S. Makino, Y. Totsuka, and S. Yoshida.** 2001. Desmoplakin as a specific marker of lymphatic vessels. Microvasc. Res. **61:**40–48.
13. **Enholm, B., K. Paavonen, A. Ristimaki, V. Kumar, Y. Gunji, J. Klefstrom, L. Kivinen, M. Laiho, B. Olofsson, V. Joukov, U. Eriksson, and K. Alitalo.** 1997. Comparison of VEGF, VEGF-B, VEGF-C and Ang-1 mRNA regulation by serum, growth factors, oncoproteins and hypoxia. Oncogene **14:**2475–2483.
14. **Fang, J., S. L. Dagenais, R. P. Erickson, M. F. Arlt, M. W. Glynn, J. L. Gorski, L. H. Seaver, and T. W. Glover.** 2000. Mutations in FOXC2 (MFH-

1), a forkhead family transcription factor, are responsible for the hereditary lymphedema-distichiasis syndrome. Am. J. Hum. Genet. **67:**1382–1388.
15. **Farnsworth, R. H., M. G. Achen, and S. A. Stacker.** 2006. Lymphatic endothelium: an important interactive surface for malignant cells. Pulm. Pharmacol. Ther. **19:**51–60.
16. **Finegold, D. N., M. A. Kimak, E. C. Lawrence, K. L. Levinson, E. M. Cherniske, B. R. Pober, J. W. Dunlap, and R. E. Ferrell.** 2001. Truncating mutations in FOXC2 cause multiple lymphedema syndromes. Hum. Mol. Genet. **10:**1185–1189.
17. **Garrafa, E., L. Trainini, A. Benetti, E. Saba, L. Fezzardi, B. Lorusso, P. Borghetti, T. Bottio, E. Ceri, N. Portolani, S. Bonardelli, S. M. Giulini, G. Annibale, A. Corradi, L. Imberti, and A. Caruso.** 2005. Isolation, purification, and heterogeneity of human lymphatic endothelial cells from different tissues. Lymphology **38:**159–166.
18. **Gerli, R., L. Ibba, and C. Fruschelli.** 1990. A fibrillar elastic apparatus around human lymph capillaries. Anat. Embryol. **181:**281–286.
19. **Hirakawa, S., Y. K. Hong, N. Harvey, V. Schacht, K. Matsuda, T. Libermann, and M. Detmar.** 2003. Identification of vascular lineage-specific genes by transcriptional profiling of isolated blood vascular and lymphatic endothelial cells. Am. J. Pathol. **162:**575–586.
20. **Irrthum, A., K. Devriendt, D. Chitayat, G. Matthijs, C. Glade, P. M. Steijlen, J. P. Fryns, M. A. Van Steensel, and M. Vikkula.** 2003. Mutations in the transcription factor gene SOX18 underlie recessive and dominant forms of hypotrichosis-lymphedema telangiectasia. Am. J. Hum. Genet. **72:**1470–1478.
21. **Jimenez, B., O. V. Volpert, S. E. Crawford, M. Febbraio, R. L. Silverstein, and N. Bouck.** 2000. Signals leading to apoptosis-dependent inhibition of neovascularization by thrombospondin-1. Nat. Med. **6:**41–48.
22. **Kaipainen, A., J. Korhonen, T. Mustonen, V. W. van Hinsbergh, G. H. Fang, D. Dumont, M. Breitman, and K. Alitalo.** 1995. Expression of the *fms*-like tyrosine kinase 4 gene becomes restricted to lymphatic endothelium during development. Proc. Natl. Acad. Sci. USA **92:**3566–3570.
23. **Karpanen, T., and T. Mäkinen.** 2006. Regulation of lymphangiogenesis: from cell fate determination to vessel remodeling. Exp. Cell. Res. **312:**575–583.
24. **Kriehuber, E., S. Breiteneder-Geleff, M. Groeger, A. Soleiman, S. F. Schoppmann, G. Stingl, D. Kerjaschki, and D. Maurer.** 2001. Isolation and characterization of dermal lymphatic and blood endothelial cells reveal stable and functionally specialized cell lineages. J. Exp. Med. **194:**797–808.
25. **Lorenzon, P., E. Vecile, E. Nardon, E. Ferrero, J. M. Harlan, F. Tedesco, and A. Dobrina.** 1998. Endothelial cell E- and P-selectin and vascular cell adhesion molecole-1 function as signaling receptor. J. Cell Biol. **142:**1381–1391.
26. **Mäkinen, T., C. Norrmén, and T. V. Petrova.** 2007. Molecular mechanisms of lymphatic vascular development. Cell. Mol. Life Sci. **64:**1915–1929.
27. **Mancardi, S., G. Stanta, N. Dusetti, M. Bestagno, L. Jussila, M. Zweyer, G. Lunazzi, D. Dumont, K. Alitalo, and O. R. Burrone.** 1999. Lymphatic endothelial tumors induced by intraperitoneal injection of incomplete Freund's adjuvant. Exp. Cell. Res. **246:**368–375.
28. **Negrini, D., A. Passi, G. de Luca, and G. Miserocchi.** 1996. Pulmonary interstitial pressure and proteoglycans during development of pulmonary edema. Am. J. Physiol. **270:**2000–2007.
29. **Negrini, D., O. Tenstad, A. Passi, and H. Wiig.** 2006. Differential degradation of matrix proteoglycans and edema development in rabbit lung. Am. J. Physiol. Lung Cell. Mol. Physiol. **290:**470–477.
30. **Pelosi, P., P. R. Rocco, D. Negrini, and A. Passi.** 2007. The extracellular matrix of the lung and its role in edema formation. An. Acad. Bras. Cienc. **79:**285–297.
31. **Petrova, T. V., T. Karpanen, C. Norrmen, R. Mellor, T. Tamakoshi, D. N. Finegold, R. Ferrell, D. Kerjaschki, P. Mortimer, S. Yla-Herttuala, N. Miura, and A. Alitalo.** 2004. Defective valves and abnormal mural cell recruitment underlie lymphatic vascular failure in lymphedema distichiasis. Nat. Med. **10:**974–981.
32. **Petrova, T. V., T. Makinen, T. P. Makela, J. Saarela, I. Virtanen, R. E. Ferrell, D. N. Finegold, D. Kerjaschki, S. Ylä-Herttuala, and K. Alitalo.** 2002. Lymphatic endothelial reprogramming of vascular endothelial cells by the prox-1 homeobox transcription factor. EMBO J. **21:**4593–4599.
33. **Podgrabinska, S., P. Braun, P. Velasco, B. Kloos, M. S. Pepper, and M. Skobe.** 2002. Molecular characterization of lymphatic endothelial cells. Proc. Natl. Acad. Sci. USA **99:**16069–16074.
34. **Pure, E., and C. A. Cuff.** 2001. A crucial role for CD44 in inflammation. Trends Mol. Med. **7:**213–221.
35. **Solito, R., C. Alessandrini, M. Fruschelli, A. M. Pucci, and R. Gerli.** 1997. An immunological correlation between the anchoring filaments of initial lymph vessels and the neighboring elastic fibers: a unified morphofunctional concept. Lymphology **30:**194–202.
36. **Spessotto, P., M. Cervi, M. T. Mucignat, G. Mungiguerra, I. Sartoretto, R. Doliana, and A. Colombatti.** 2003. Beta 1 integrin-dependent cell adhesion to EMILIN-1 is mediated by the gC1q domain. J. Biol. Chem. **278:**6170–6177.
37. **Spessotto, P., R. Bulla, C. Danussi, O. Radillo, M. Cervi, G. Monami, F. Bossi, F. Tedesco, R. Doliana, and A. Colombatti.** 2006. EMILIN1 represents a major stromal element determining human trophoblast invasion of the uterine wall. J. Cell Sci. **119:**4574–4584.
38. **Streit, M., P. Velasco, L. Riccardi, L. Spencer, L. F. Brown, L. Janes, B. Lange-Asschenfeldt, K. Yano, T. Hawighorst, L. Iruela-Arispe, and M. Detmar.** 2000. Thrombospondin-1 suppresses wound healing and granulation tissue formation in the skin of transgenic mice. EMBO J. **19:**3272–3282.
39. **Sugaya, M., T. Watanabe, A. Yang, M. F. Starost, H. Kobayashi, A. M. Atkins, D. L. Borris, E. A. Hanan, D. Schimel, M. A. Bryant, N. Roberts, M. Skobe, K. A. Staskus, P. Kaldis, and A. Blauvelt.** 2005. Lymphatic dysfunction in transgenic mice expressing KSHV k-cyclin under the control of the VEGFR-3 promoter. Blood **105:**2356–2363.
40. **Swartz, M. A., and M. Skobe.** 2001. Lymphatic function, lymphangiogenesis, and cancer metastasis. Microsc. Res. Technol. **55:**92–99.
41. **Tammela, T., T. V. Petrova, and K. Alitalo.** 2005. Molecular lymphangiogenesis: new players. Trends Cell. Biol. **15:**434–441.
42. **Tolsma, S. S., O. V. Volpert, D. J. Good, W. A. Frazier, P. J. Polverini, and N. Bouck.** 1993. Peptides derived from two separate domains of the matrix protein thrombospondin-1 have anti-angiogenic activity. J. Cell Biol. **122:**497–511.
43. **Volpert, O. V., J. Lawler, and N. P. Bouck.** 1998. A human fibrosarcoma inhibits systemic angiogenesis and the growth of experimental metastases via thrombospondin-1. Proc. Natl. Acad. Sci. USA **95:**6343–6348.
44. **Wigle, J. T., N. Harvey, M. Detmar, I. Lagutina, G. Grosveld, M. D. Gunn, D. G. Jackson, and G. Oliver.** 2002. An essential role for Prox1 in the induction of the lymphatic endothelial cell phenotype. EMBO J. **21:**1505–1513.
45. **Witte, M. H., M. J. Bernas, C. P. Martin, and C. L. Witte.** 2001. Lymphangiogenesis and lymphangiodysplasia: from molecular to clinical lymphology. Microsc. Res. Technol. **55:**122–145.
46. **Yuan, L., D. Moyon, L. Pardanaud, C. Bréant, M. J. Karkkainen, K. Alitalo, and A. Eichmann.** 2002. Abnormal lymphatic vessel development in neuropilin 2 mutant mice. Development **129:**4797–4806.
47. **Zacchigna, L., C. Vecchione, A. Notte, M. Cordenonsi, S. Dupont, S. Maretto, G. Cifelli, A. Ferrari, A. Maffei, C. Fabbro, P. Braghetta, G. Marino, G. Selvetella, A. Aretini, C. Colonnese, U. Bettarini, G. Russo, S. Soligo, M. Adorno, P. Bonaldo, D. Volpin, S. Piccolo, G. Lembo, and G. M. Bressan.** 2006. Emilin1 links TGF-beta maturation to blood pressure homeostasis. Cell **124:**929–942.
48. **Zanetti, M., P. Braghetta, P. Sabatelli, I. Mura, R. Doliana, A. Colombatti, D. Volpin, P. Bonaldo, and G. M. Bressan.** 2004. EMILIN-1 deficiency induces elastogenesis and vascular cell defects. Mol. Cell. Biol. **24:**638–650.